Surv Geophys
DOI 10.1007/s10712-011-9171-x

An Assessment of Two-Dimensional Past Sea Level Reconstructions Over 1950–2009 Based on Tide-Gauge Data and Different Input Sea Level Grids

B. Meyssignac · M. Becker · W. Llovel · A. Cazenave

Received: 8 August 2011 / Accepted: 23 December 2011

Abstract We compare different past sea level reconstructions over the 1950–2009 time span using the Empirical Orthogonal Function (EOF) approach. The reconstructions are based on 91 long (up to 60 years) but sparsely distributed tide-gauge records and gridded sea level data from two numerical ocean models over 1958–2007 (the DRAKKAR/NEMO model without data assimilation and the simple ocean data assimilation ocean reanalysis-SODA-) and satellite altimetry data over 1993–2009. We find that the reconstructed global mean sea level computed over the ~60-year-long time span little depends on the input spatial grids. This is unlike the regional variability maps that appear very sensitive to the considered input spatial grids. Using the DRAKKAR/NEMO model, we test the influence of the period covered by the input spatial grids and the number of EOFs modes used to reconstruct sea level. Comparing with tide-gauge records not used in the reconstruction, we determine optimal values for these two parameters. As suggested by previous studies, the longer the time span covered by the spatial grids, the better the fit with unused tide gauges. Comparison of the reconstructed regional trends over 1950–2009 based on the two ocean models and satellite altimetry grids shows good agreement in the tropics and substantial differences in the mid and high latitude regions, and in western boundary current areas as well. The reconstructed spatial variability seems very sensitive to the input spatial information. No clear best case emerges. Thus, using the longest available model-based spatial functions will not necessarily give the most realistic results as it will be much dependent on the quality of the model (and its associated forcing). Altimetry-based reconstructions

B. Meyssignac (✉) · M. Becker · W. Llovel · A. Cazenave
Laboratoire d'Etudes en Géophysique et Océanographie Spatiale, Toulouse, France
e-mail: benoit.meyssignac@legos.obs-mip.fr

Present Address:
M. Becker
ESPACE-DEV UMR 228 IRD/UM2/UR/UAG, Université Antilles-Guyane, Cayenne, France

Present Address:
W. Llovel
Jet Propulsion Laboratory, Pasadena, CA, USA

Published online: 24 January 2012

(with 17-year long input grids) give results somewhat similar to cases with longer model grids. It is likely that better representation of the sea level regional variability by satellite altimetry compensates the shorter input grids length. While waiting for much longer altimetry records, improved past sea level reconstructions may be obtained by averaging an ensemble of different model-based reconstructions, as classically done in climate modelling. Here, we present such a 'mean' reconstruction (with associated uncertainty) based on averaging the three individual reconstructions discussed above.

Keywords Reconstructed sea level · Tide gauges · Satellite altimetry · Ocean general circulation models · Spatial variability

1 Introduction

Sea level rise is a critical issue of global climate change because of its potential huge impacts on coastal areas (Nicholls 2010). Tide-gauge measurements indicate that, during the twentieth century, the mean rate of sea level rise has been on the order of 1.6–1.8 mm/year (Church and White 2006, 2011; Jevrejeva et al. 2006, 2008; Holgate 2007; Woppelmann et al. 2009; Wenzel and Schroeter 2010; Ray and Douglas 2011). Since the beginning of the 1990s, sea level is measured by high-precision satellite altimetry with global coverage. The satellite observations have shown that sea level does not rise uniformly but displays characteristic spatial trend patterns (see Fig. 1 showing the altimetry-based spatial trend patterns over 1993–2009, with a uniform global mean trend of 3.2 mm/year removed). For example, since early 1993 (the beginning of the high-precision altimetry era), the rate of sea level rise in the western tropical Pacific, southern Ocean and part of the north Atlantic has been 3–4 times faster than the global mean rise of

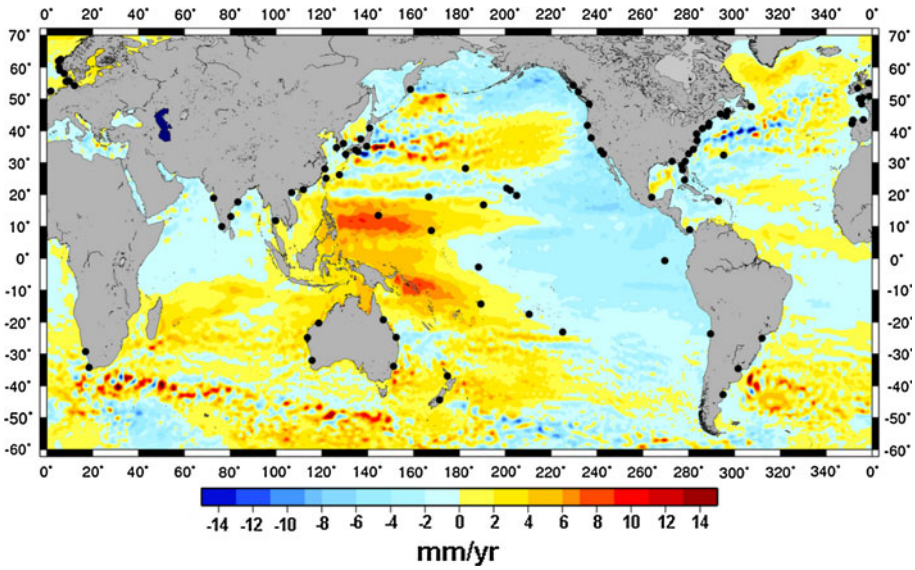

Fig. 1 Spatial trend patterns in sea level from satellite altimetry (1993–2009). A uniform trend of 3.2 mm/year has been removed. Locations of the 91 tide gauges used for the reconstructions are indicated by *black dots*

3.2 ± 0.5 mm/year (Ablain et al. 2009; Nerem et al. 2010). In other regions (e.g., the eastern Pacific), the rate has been slower. These large deviations from the global mean show the importance of estimating and understanding the regional variability of sea level change. This is indeed essential when assessing the potential impacts of sea level rise in coastal areas.

While a number of recent studies focussed on the global mean rise and its causes for the past few decades or altimetry era (e.g., Cazenave and Llovel 2010; Moore et al. 2011; Church et al. 2011), less attention has been given to the regional variability. It is known from previous studies based either on in situ hydrographic data or ocean general circulation models (OGCMs) that the regional variability in sea level is mainly of steric origin (i.e. due to thermal expansion and salinity changes) (Levitus et al. 2005; Lombard et al. 2005; Wunsch et al. 2007; Kohl and Stammer 2008). Other phenomena such as circulation changes due to polar ice melt (Stammer 2008; Stammer et al. 2011) or gravitational effects and visco-elastic response of the solid Earth to last deglaciation and ongoing land ice melt also cause regional variability (e.g., Peltier 2004; Milne et al. 2009; Mitrovica et al. 2009) but corresponding signals are currently smaller than the steric one and have not yet been clearly detected.

It has been shown as well (e.g., Lombard et al. 2005; Levitus et al. 2005; Meyssignac et al. 2011a) that trend patterns in thermal expansion fluctuate with time and space in response to the main modes of variability of the climate system (El Nino-southern Oscillation/ENSO, Pacific Decadal Oscillation/PDO, North Atlantic Oscillation/NAO, Indian Ocean Dipole/IOD, etc.). Thus the high correlation between observed and steric regional variability in sea level over the altimetry era suggests that the altimetry-based spatial trend patterns are not long-lived features, but rather reflect natural modes of ocean variability. Prior to the altimetry era, there is no direct way for measuring globally the regional variability in sea level. However, different approaches can inform about the spatial sea level trend patterns over the last 5–6 decades: (1) Ocean General Circulation Models (OGCMs) and ocean reanalyses (i.e. OGCMs with data assimilation) (e.g., Carton and Giese 2008; Kohl and Stammer 2008) and (2) two-dimensional (2-D) past sea level reconstructions (e.g., Chambers et al. 2002a, b; Church et al. 2004; Berge-Nguyen et al. 2008; Llovel et al. 2009 Church and White 2011; Ray and Douglas 2011; Hamlington et al. 2011). Analysis of corresponding sea level gridded time series can inform on the spatio-temporal variability of past sea level and on the characteristic lifetime of the trend patterns. OGCMs and ocean reanalyses deduce sea level from the sum of the thermosteric (effect of temperature) and halosteric (effect of salinity) components, to which is added a small barotropic component. This allows to follow the temporal behaviour of both temperature and salinity contributions. This is unlike the sea level reconstructions that do not separate these contributions. However, being partly based on tide-gauge observations, the reconstructions may in principle carry more information on the regional variability factors than OGCMs and thus can be viewed as complementary to the latter.

The present study is dedicated to past sea level reconstructions. Its objective is to investigate the influence of the chosen spatial modes used to constrain the reconstruction and the period covered by the corresponding gridded sea level time series. For that purpose, we use three different sea level gridded products (hereafter called input grids) derived from (1) a purely physical ocean circulation model without data assimilation (DRAKKAR/NEMO ocean model, DRAKKAR Group 2007), (2) an ocean reanalysis (SODA, Carton and Giese 2008) and (3) satellite altimetry data. We show that the nature and period of the input spatial grids have strong impact on the reconstructed spatial patterns. Comparison with tide-gauge data not used in the reconstructions leads us to conclude that depending on

the region, some cases perform better than others. But no single case appears to be able to perform better at the planetary scale.

Section 2 describes the reconstruction methodology as used in previous reconstruction studies. Section 3 describes the data and input grids used in this study. Results and discussion are presented in Sects. 4 and 5.

2 Reconstruction Methodology

Several previous studies have developed past (last 50–60 years or last century) sea level reconstructions either globally (e.g., Chambers et al. 2002a, b; Church et al. 2004; Berge-Nguyen et al. 2008; Llovel et al. 2009; Church and White 2011; Hamlington et al. 2011; Ray and Douglas 2011) or regionally (e.g., Calafat and Gomis 2009; Meyssignac et al. 2011b). The method used in most previous studies (as well as in the present one) is based on the reduced optimal interpolation described by Kaplan et al. (1998, 2000). It consists of 2 steps. In the first step, an Empirical Orthogonal Function (EOF) decomposition (Preisendorfer 1988; Toumazou and Cretaux 2001) of a 2-D sea level field (generally from satellite altimetry but also from OGCMs or ocean reanalyses) is done. This decomposition allows to separate the spatially well-resolved sea level signal (here represented by a matrix H, with m lines for each spatial point and n columns for each date) into spatial modes (EOFs) and their related temporal amplitude as follows:

$$H(x, y, t) = U(x, y)\alpha(t) \tag{1}$$

In Eq. 1, $U(x, y)$ stands for the spatial modes and α(t) for their temporal amplitudes. Assuming that the spatial modes $U(x, y)$ are stationary with time, the reconstructed sea level field $H_R(x, y, t)$ covering a period (here 1950–2009) longer than the $H(x, y, t)$ fields has an EOF decomposition as follows:

$$H_R(x, y, t) = U(x, y)\alpha_R(t) \tag{2}$$

where $\alpha_R(t)$ represents the new temporal amplitudes of the EOFs over 1950–2009.

The second step consists of computing these new amplitudes over the whole period 1950–2009 using in situ (tide gauge-based) sea level records. This is done at each time step, through a least-squares procedure which gives the optimal linear combination of the EOFs that fits the tide-gauge records at the tide-gauge locations.

In the first step, the EOF modes and amplitudes of the 2-D sea level grids are computed through a singular value decomposition approach, such that:

$$H = USV^T \tag{3}$$

where $U(x, y)$ is defined as above, S is a diagonal matrix containing the singular values of H, and V represents the temporal eigenmodes. At this stage, the amplitude of the EOF modes can be simply written as $\alpha(t) = SV^T$. Conceptually, each EOF k (kth column of $U(x, y)$ multiplied by the kth line of $\alpha(t)$:$U_k(x, y).\alpha_k(t)$) is a spatio-temporal pattern of sea level variability that accounts for a percentage of the total variance of the sea level signal.

The low-order EOFs (eigenvectors of the largest singular values) explain most of the variance and contain the largest spatial scales of the signal. The higher-order EOFs contain smaller spatial scale patterns and are increasingly affected by noise. Besides, their amplitude is less well resolved by the least-squares procedure, because the sparse tide-gauges coverage does not allow resolving small-scale patterns. Consequently, to be

efficient, the sea level reconstruction uses only a subset of the M lowest-order EOFs (the optimal number of EOFs has been estimated by comparison of the reconstructed sea level with observations; see below).

The data matrix H can be written as follows:

$$H_M = U_M(x, y)\alpha(t) \tag{4}$$

where $\alpha(t) = S_M V_M^T$ is the matrix of the amplitude of the M lowest EOFs. Following Kaplan et al. (2000), in the second step, the amplitude at each time step over the time span of in situ records is obtained by minimizing the cost function:

$$S(\alpha) = \left(PU_M\alpha - H^0\right)^T R^{-1}\left(PU_M\alpha - H^0\right) + \alpha^T\Lambda^{-1}\alpha \tag{5}$$

In Eq. 5, H^0 is the in situ (tide gauge-based) observed sea level, P is a projection matrix equal to 1 when and where in situ data are available and 0 otherwise. Λ is a diagonal matrix of the largest eigen-values of the covariance matrix. The term $\alpha^T\Lambda^{-1}\alpha$ represents a constraint on the EOF spectrum of the solution. It prevents the least-squares procedure to be contaminated by remaining high-frequency noise (it filters out non-significant solutions that display too much variance at grid points without nearby observations). R is the error covariance matrix. It is given by $R = PU_{N-M}\Lambda_{N-M}U_{N-M}^T P^T + D$. The first term of R contains the covariance of the truncated modes (the index 'N–M' indicates the omitted eigenvectors and eigenvalues). It accounts for errors due to the truncation of the set of EOFs to the first M EOFs. D accounts for the instrumental error. We have assumed here a spatially uncorrelated instrumental error so D is the identity matrix multiplied by the instrumental error variance. Amplitudes of the variance used for each reconstruction are indicated below.

When Eq. 5 is solved, it provides the reconstructed amplitude α_R of the EOFs. The least-squares inversion gives an analytical expression of α_R as follows:

$$\alpha_R(t) = QU_M^T P^T R^{-1} H^0(t) \tag{6}$$

$$\text{with} \quad Q = \left(U_M^T P^T R^{-1} P U_M + \Lambda^{-1}\right)^{-1}$$

When solving Eq. 6, two problems further arise. First, because tide-gauge data are expressed relative to their own local datum that is not cross-referenced over the globe, the solution may not necessarily be consistent with the 2-D sea level grid reference surface (from OGCM or altimetry data). To cope with this problem, Church et al. (2004) solved Eq. 6 for changes in α_R between adjacent time steps. It is also the procedure applied in the present study. Instead of computing α_R, we compute $\Delta\alpha_R(t_n) = \alpha_R(t_n) - \alpha_R(t_{n-1})$ thanks to the equation $\Delta\alpha_R = QU_M^T P^T R^{-1}\Delta H^0$. This provides for each time step, the changes in amplitude of α_R which are independent from the tide-gauge local references. Then α_R itself is recovered by summing backward in time $\Delta\alpha_R$ and equalizing the mean amplitude of α_R to the mean amplitude of α (amplitude of the EOF of the OGCM or altimetry data) over the common period. With this procedure, the consistency between the reference surfaces of tide gauges and 2-D sea level grids (from OGCM or altimetry) is ensured.

Another issue in global sea level reconstructions is the large spatially averaged sea level signal (of about 1.7–1.8 mm/year since about 1950; e.g., Church and White 2006, 2011; Woppelmann et al. 2009). This signal, which is contained in the tide-gauge data, is hard to capture and recover from a truncated set of orthogonal EOFs deduced from 2-D gridded sea level (see Christiansen et al. 2010). Hence, following Church et al. (2004) and the results of Christiansen et al. (2010), a spatially uniform EOF (also called EOF0, as in

Church et al. 2004) is added to the set of EOFs in order to represent the time-varying spatially averaged signal of the global ocean in the past. An advantage of this procedure is to avoid pouring the strong past global-averaged sea level signal in different EOFs and perturbing the reconstruction process (e.g., Kaplan et al. 2000).

The final reconstructed gridded sea level is obtained by multiplying the set of M EOFs plus the EOF0 with their reconstructed amplitude:

$$H_R = U_M(x, y).\alpha_R(t) \tag{7}$$

Other authors have performed past sea level reconstructions using different basis functions. For example, Hamlington et al. (2011) use cyclostationary EOFs as basis functions. Unlike classical EOFs, cyclostationary EOFs are periodic and can capture cyclostationary signals such as the annual signal into a single mode. This enables reconstructing the annual signal along with the interannual signal through a unique process.

3 Data Sets Used in this Study

In this study, we used a set of 91 tide-gauge records selected from the Permanent Service for Mean Sea Level (PSMSL) database (http://www.psmsl.org/about_us/news/2010/new_website.php, Woodworth and Player 2003). These records were optimally interpolated (as explained above) with EOFs computed from three different input grids: (1) the ORCA025-B83 run of the DRAKKAR/NEMO model (Barnier et al. 2006; Dussin et al. 2009), (2) the SODA ocean reanalysis (Carton and Giese 2008) and (3) the 17-year long satellite altimetry data set. These data sets are described here after in this section.

3.1 Tide-Gauge Records

We use monthly mean sea level data from the Revised Local Reference (RLR) tide-gauge records of the PSMSL (downloaded in May 2011). A very careful selection of sites has been realized. From the whole set of data available, we consider records at least 35-year long over 1950–2009. Compared with the 99 records considered in Llovel et al. (2009), here we use only 91 records, deleting a number of tide-gauge records with suspect behaviour. In effect, for a number of reasons, gaps and discontinuities may affect the tide-gauge time series (e.g., changes in instrumentation, earthquakes or any other natural or anthropogenic factors). When small gaps (<3 consecutive years) are observed in the tide-gauge record, we reintroduced missing data by linearly interpolating the time series. Outliers were detected using the Rosner's test (Rosner 1975) and removed. Annual and semi-annual cycles were removed (before gap-filling) through a least-squares fit of 12-month and 6-month period sinusoids. At a few sites, recent data (i.e. up to 2009) are lacking in the PSMSL data base. Thus, we completed these tide-gauge time series using altimetry data (22 sites are concerned). To do so, the following constraints have been considered: (1) availability of altimetry measurement at less than 1 degree from the tide-gauge position; and (2) overlapping period of at least 5 years between tide-gauge records and altimetry data (this overlap length was deduced from the Bonnet's formula, Bonett and Wright (2000), in order to insure a correlation >0.9 between the two data sets). The closest altimetry record to the tide-gauge position has been used to complete the tide-gauge sea level time series. We corrected the tide-gauge time series for the inverted barometer response of sea level to atmospheric loading using surface pressure fields from the National

Centres for Environmental Prediction (NCEP; Kalnay et al. 1996, http://www.ncep.noaa.gov/). Tide-gauge data were also corrected for the Glacial Isostatic Adjustment (GIA) effect using the ICE5G-VM2 model from Peltier (2004). As we focus here on interannual to multidecadal time scales, we averaged monthly tide-gauge time series to obtain annual averages. Figure 1 shows the distribution of the tide-gauge sites used in this study (superimposed to the altimetry sea level trend map over 1993–2009). Name, location and data length of the 91 tide gauges are summarized in Table 1. Tide-gauge records completed by altimetry data are those that end before 2009.

3.2 Input Sea Level Grids

To compute the EOFs needed to reconstruct past sea level, three input sea level grids were considered: from the DRAKKAR/NEMO OGCM (without data assimilation) over 1958–2007, from the SODA ocean reanalysis over 1958–2007 and the altimetry-based gridded sea level over 1993–2009. These data sets are briefly presented below.

3.2.1 The DRAKKAR/NEMO Ocean General Circulation Model

The DRAKKAR NEMO model is based on the free surface ocean circulation model NEMO version 2.3 (Madec 2008). We used the outputs of the ORCA025-B83 model configuration (Barnier et al. 2006; Dussin et al. 2009; Penduff et al. 2010). This is a global eddy-admitting ocean/sea-ice simulation that does not assimilate any observational data (e.g., satellite altimetry or in situ hydrographic data). It is very close to the simulation ORCA025-G70 analysed and proved to be consistent with altimetry by Lombard et al. (2009). It has the same horizontal and vertical resolution (46 levels with steps from 6 m at the surface to 250 m at the bottom). The main difference with ORCA025-G70 is the forcing function. ORCA025-B83 is forced by the more realistic hybrid 'DRAKKAR forcing set 4.1' surface forcing described in details by Brodeau et al. (2010). This forcing is based on the CORE data set assembled by W. Large (Large and Yeager 2004), the ECMWF (European Centre for Medium-Range Weather Forecast) ERA 40 reanalysis (Uppala et al. 2005) and the ECMWF operational analyses for the recent years. The simulation was started on the 1st January 1958, with initial conditions for salinity and temperature derived from the Levitus et al. (2005) data set for middle and low latitudes, from the Polar Science Center Hydrographic climatology for the high latitudes (Steele et al. 2001) and from the MEDATLAS climatology (Jourdan et al. 1998) for the Mediterranean sea. Initial conditions for sea-ice were taken from the month of January of the 10th year of ORCA025-G45b (a previous run with a climatological CORE forcing).

In the ORCA025-B83 simulation, the time-varying globally averaged sea level is not properly reproduced because it has been simulated on the basis of the Boussinesq approximation which enforces the total ocean volume (rather than mass) to remain constant. In particular, as shown by Greatbatch (1994), no spatially uniform steric sea level changes can be reproduced by such a model (even though the free surface evolution allows simulating correctly the net freshwater surface fluxes at both regional and global scale). For this reason, prior to the computation of the EOFs, we removed the time-varying globally averaged sea level from each sea surface height time series of the simulation. By doing this, we get a consistent set of EOFs, which are representative of the regional variability in sea level. Indeed, as shown by Greatbatch (1994) (apart from the unrealistic global uniform sea level changes), regional variations are properly reproduced by such a free surface model. Concerning the reconstruction process, the fact that the set of EOFs does not

Table 1 Name, location (degrees of latitude North, and longitude East, being positive), length and percentage of gaps of the tide-gauge series selected from the PSMSL for the reconstructions

ID	Station name	Location		Years of data		Percentage of gaps (max. gap size in months)	Altimetry data used for supplemented the time series or filling the gap
		Longitude	Latitude	Start	End		
1	North Shields	−1.43	55.00	1950	2009	15% (43)	–
2	St. Petersburg	−82.62	27.77	1950	2009	0% (0)	–
3	St. Georges/Esso Pier	−64.70	32.37	1950	2009	9% (41)	–
4	Alesund	6.15	62.47	1951	2009	2% (2)	–
5	Maloy	5.12	61.93	1950	2009	7% (26)	–
6	Bergen	5.30	60.40	1950	2009	3% (6)	–
7	Stavanger	5.73	58.97	1950	2009	3% (16)	–
8	Tregde	7.57	58.00	1950	2009	2% (6)	–
9	Warnemunde 2	12.08	54.18	1950	2009	0% (2)	–
10	Lowestoft	1.75	52.47	1955	2009	6% (12)	–
11	Portsmouth	−1.12	50.80	1961	2009	4% (6)	–
12	Devonport	−4.18	50.37	1961	2009	4% (4)	–
13	Newlyn	−5.55	50.10	1950	2009	1% (4)	–
14	Brest	−4.50	48.38	1952	2009	0% (1)	–
15	Santander I	−3.80	43.47	1950	2009	3% (3)	–
16	La Coruna I	−8.40	43.37	1950	2009	3% (2)	–
17	Vigo	−8.73	42.23	1950	2009	1% (4)	–
18	Port Nolloth	16.87	−29.25	1959	2009	23% (72)	–
19	Simons Bay	18.43	−34.18	1957	2009	17% (49)	–
20	Ko Lak	99.82	11.80	1950	2009	4% (12)	–
21	Zhapo	111.83	21.58	1959	2009	1% (1)	–
22	Kanmen	121.28	28.08	1959	2009	1% (2)	–
23	Petropavlovsk-Kamchatsky	158.65	52.98	1957	2009	0% (1)	–
24	Aburatsubo	139.62	35.15	1950	2009	1% (1)	–
25	Kushimoto	135.78	33.47	1957	2009	1% (2)	–
26	Komatsushima	134.58	34.00	1958	2009	1% (3)	–
27	Misumi	130.45	32.62	1957	2009	3% (5)	–
28	Naha	127.67	26.22	1966	2009	0% (1)	–
29	Wajima	136.90	37.40	1950	2009	4% (12)	–
30	Asamushi	140.87	40.90	1954	2009	1% (5)	–
31	Townsville I	146.83	−19.25	1959	2009	0% (1)	–
32	Bundaberg, Burnett Heads	152.38	−24.77	1966	2009	2% (4)	–
33	Fremantle	115.75	−32.07	1950	2009	2% (3)	–
34	Carnarvon	113.65	−24.90	1965	2009	13% (38)	–
35	Port Hedland	118.57	−20.32	1966	2009	6% (10)	–
36	Guam	144.65	13.43	1950	2009	6% (14)	–
37	Kwajalein	167.73	8.73	1950	2009	2% (2)	–
38	Wake Island	166.62	19.28	1950	2009	7% (17)	–

Table 1 continued

ID	Station name	Location		Years of data		Percentage of gaps (max. gap size in months)	Altimetry data used for supplemented the time series or filling the gap
		Longitude	Latitude	Start	End		
39	Pago Pago	−170.68	−14.28	1950	2009	7% (24)	–
40	Midway Island	−177.37	28.22	1950	2009	6% (14)	–
41	Nawiliwili Bay, Kauai Island	−159.35	21.97	1955	2009	1% (3)	–
42	Honolulu	−157.87	21.32	1950	2009	0% (0)	–
43	Hilo, Hawaii Island	−155.07	19.73	1950	2009	0% (0)	–
44	Papeete-B, Soc.IS.	−149.57	−17.53	1975	2009	2% (7)	–
45	Prince Rupert	−130.33	54.32	1950	2009	1% (2)	–
46	Bella Bella	−128.13	52.17	1961	2009	3% (2)	–
47	Victoria	−123.37	48.42	1950	2009	1% (1)	–
48	Crescent City	−124.20	41.75	1950	2009	2% (9)	–
49	San Francisco	−122.47	37.80	1950	2009	0% (0)	–
50	Los Angeles	−118.27	33.72	1950	2009	2% (6)	–
51	San Diego	−117.17	32.72	1950	2009	2% (9)	–
52	Veracruz	−96.12	19.18	1953	2009	7% (27)	–
53	Magueyes Island	−67.05	17.97	1955	2009	4% (12)	–
54	Pensacola	−87.22	30.40	1950	2009	2% (5)	–
55	Cedar Key II	−83.03	29.13	1950	2009	6% (20)	–
56	Key West	−81.80	24.55	1950	2009	1% (8)	–
57	Charleston I	−79.93	32.78	1950	2009	0% (0)	–
58	Wilmington	−77.95	34.23	1950	2009	2% (6)	–
59	Hampton Roads	−76.33	36.95	1950	2009	0% (0)	–
60	Baltimore	−76.58	39.27	1950	2009	2% (12)	–
61	New York	−74.02	40.70	1950	2009	1% (4)	–
62	Newport	−71.33	41.50	1950	2009	2% (10)	–
63	Boston	−71.05	42.35	1950	2009	1% (5)	–
64	Halifax	−63.58	44.67	1950	2009	3% (4)	–
65	Charlottetown	−63.12	46.23	1950	2009	6% (4)	–
66	St. Johns, Nfld.	−52.72	47.57	1957	2009	8% (36)	–
67	Sydney, Fort Denison 2	151.23	−33.85	1950	2009	0% (2)	–
68	Saint John, N.B.	−66.07	45.27	1950	1999	6% (5)	Yes
69	Puerto Madryn	−65.03	−42.77	1957	2000	10% (39)	Yes
70	Mumbai/ Bombay	72.83	18.92	1950	1994	2% (4)	Yes
71	Balboa	−79.57	8.97	1950	2003	1% (3)	Yes
72	Auckland II	174.77	−36.85	1950	2000	3% (6)	Yes
73	Mayport	−81.43	30.40	1950	2000	0% (2)	Yes
74	Lyttelton II	171.27	−44.40	1950	2000	10% (47)	Yes
75	Dublin	−6.22	53.35	1950	2001	1% (3)	Yes

Table 1 continued

ID	Station name	Location		Years of data		Percentage of gaps (max. gap size in months)	Altimetry data used for supplemented the time series or filling the gap
		Longitude	Latitude	Start	End		
76	Hondau	106.80	20.67	1957	2001	0% (1)	Yes
77	Johnston Island	−169.52	16.75	1950	2003	5% (15)	Yes
78	Rikitea	−134.95	−23.13	1969	2003	6% (7)	Yes
79	Fredericia	9.77	55.57	1950	2006	2% (3)	Yes
80	Esbjerg	8.43	55.47	1950	2006	3% (12)	Yes
81	Cananeia	−47.93	−25.02	1954	2006	3% (17)	Yes
82	Santa Cruz	−90.32	−0.75	1978	2006	4% (10)	Yes
83	Cochin (Willingdon IS.)	76.27	9.97	1950	2007	8% (12)	Yes
84	Chennai/Madras	80.30	13.10	1952	2007	10% (24)	Yes
85	Vishakhapatnam	83.28	17.68	1950	2007	16% (39)	Yes
86	Mokpo	126.40	34.78	1960	2009	1% (1)	–
87	Pohang	129.40	36.02	1972	2009	0% (1)	Yes
88	Keelung II	121.73	25.13	1956	1995	1% (7)	Yes
89	Antofagasta 2	−70.40	−23.65	1950	2006	7% (8)	Yes
90	Palermo	−58.36	−34.60	1950	2009	0% (0)	–
91	Kanton	−171.72	−2.80	1950	2006	15% (45)	Yes

contain any globally uniform sea level component is not an issue because an extra EOF (the globally uniform EOF called EOF0, see Sect. 2) is added to the set of EOFs to capture from the tide-gauge records the missing time-varying uniform sea level (see Sect. 2 for more details). The spatial sea level trend patterns over 1958–2007 from the DRAKKAR/ NEMO/ ORCA025-B83 model are presented in Fig. 2a.

3.2.2 The SODA Ocean Reanalysis

In this study, we also used the ocean reanalysis SODA 2.0.2 that span over the period 1958 to 2007. This reanalysis is based on an optimal interpolation described by Carton and Giese (2008). The ocean general circulation model, POP2.0.1 (see Carton and Giese 2008, for details), has a horizontal resolution of 0.4° in longitude and 0.25° in latitude, and 40 vertical levels with a resolution of about 10 m in the upper 100 m. For this study, we used the monthly mean oceanic variables interpolated on a horizontal grid of 0.5°× 0.5°. In SODA 2.0.2, POP2.0.1 is forced by ERA-40 daily wind stresses and heat fluxes. It assimilates hydrographic data from the WOD05 hydrographic data base (Levitus et al. 2005), but it does not assimilate satellite altimetry data. Sea level outputs are computed diagnostically using a linearized continuity equation valid for small ratios of sea level to fluid depth (Carton and Giese 2008).

The spatial sea level trend patterns over 1958–2007 from the SODA reanalysis are presented in Fig. 2b.

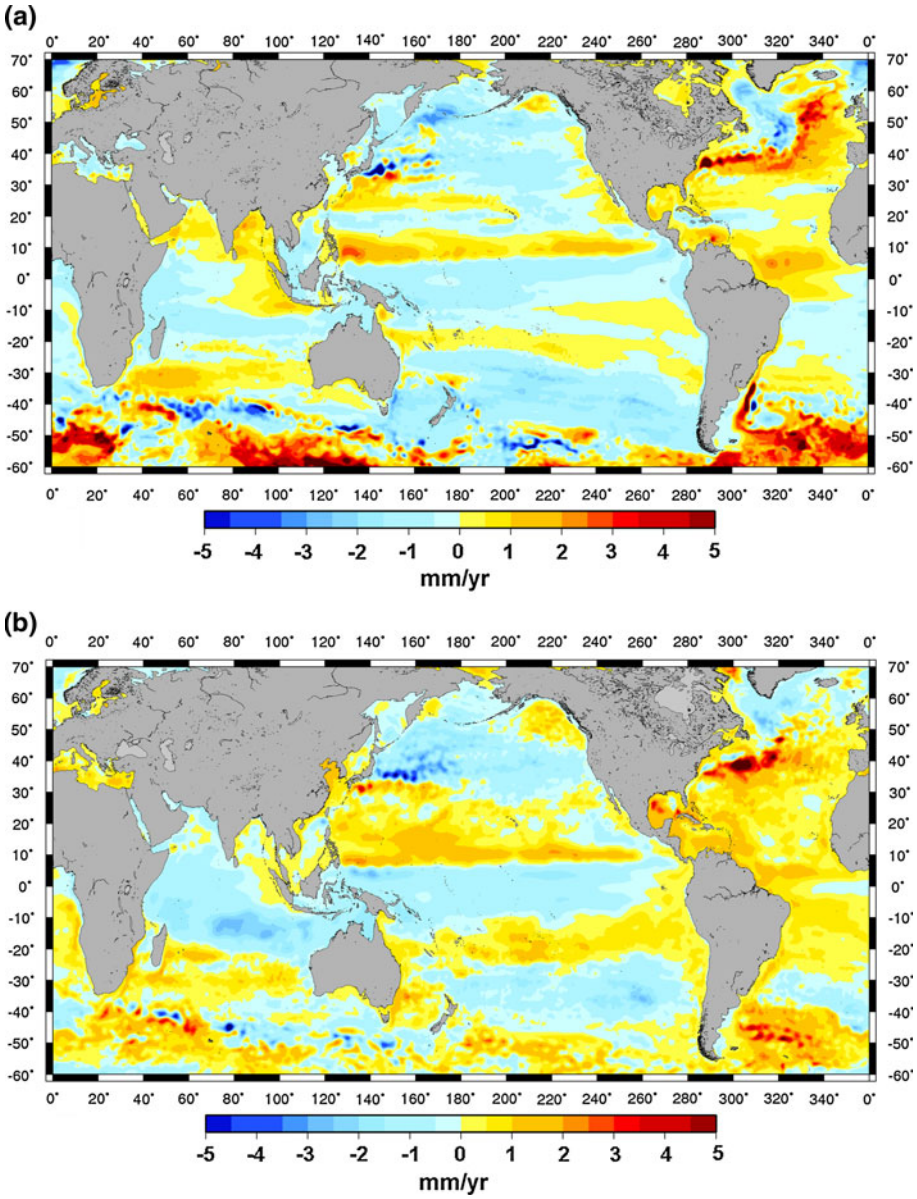

Fig. 2 Spatial trend patterns in sea level over 1958–2007 from **a** the DRAKKAR/NEMO ocean model and **b** the SODA reanalysis

3.2.3 The Altimetry Data Set

For the altimetry data, we used the DT-MSLA "Ref" series provided by Collecte Localisation Satellite (CLS; http://www.aviso.oceanobs.com/en/data/products/sea-surface-height-products/global/msla/index.html). This data set was used over the time span from January 1993 to December 2009. It is available as 1/4° × 1/4° Mercator projection grids at weekly

intervals. The DT-MSLA "Ref" series are based on the combination of several altimetry missions, namely: Topex/Poseidon (T/P), Jason-1 and 2, Envisat, and ERS-1 and ERS-2. It is a global homogenous inter-calibrated data set based on global crossover adjustment using T/P and then Jason-1 as reference missions. Moreover, the use of a recently updated orbit solution for Jason-1 and T/P (GSFC—Goddard Space Flight Center-orbit computed with the ITRF2005 terrestrial reference frame; Altamimi et al. 2007) allows to remove previous heterogeneity between global hemispheric mean sea level trends (Ablain et al. 2009). Usual geophysical corrections are applied: solid Earth and ocean tides, wet and dry troposphere, ionosphere (see Ablain et al. 2009 for more details) and inverted barometer (Carrere and Lyard 2003) corrections.

4 2-D Reconstructed Sea Level Over 1950–2009

We reconstructed 2-D sea level grids at yearly intervals over 1950–2009 using the three input sea level grids (DRAKKAR/NEMO, SODA and altimetry) described above. The same area (50°S to 70°N) was considered for each input sea level grids to ensure consistency between the reconstructions. The input sea level grids were also yearly averaged before the reconstruction process because here we are mostly interested in the interannual to multidecadal timescales. Thus, all reconstructions are based on yearly data sets.

For reconstructions based on altimetry, we considered an instrumental error variance of 4 cm^2 to compute the error covariance matrix (see Sect. 2). For reconstructions based on OGCM, there is no instrumental error but instead we consider a data error. The data error has been derived from the variance of the differences between the OGCM and the altimetry yearly data sets over their overlapping period 1993–2007. This gives a data error variance of 15.2 cm^2 for SODA and 10.9 cm^2 for DRAKKAR. These values are introduced in the error covariance matrix for the OGCM-based reconstructions.

Several reconstructions were computed to estimate the sensitivity of the reconstructed sea level with respect to two key points of the reconstruction process: (1) the number of EOF modes used in the reconstruction and (2) the period covered by the input grids used to compute the EOFs. All together, 87 different reconstructions were produced: 42 reconstructions for the DRAKKAR and SODA cases (6 series of 7 reconstructions based on 10, 15, 20, 25, 30 and 35 modes) with EOFs computed over 7 different time spans of the OGCM runs: 50 years (1958–2007), 43 years (1965–2007), 40 years (1968–2007), 38 years (1970–2007), 30 years (1978–2007), 28 years (1980–2007), and 20 years (1988–2007), plus 3 reconstructions for the altimetry cases based on 10, 15 and 17 modes, with EOFs computed over the 17-year-long time span.

4.1 Spatial trend Patterns and Modes of Variability (EOFs) of the Reconstructed Sea Level Over 1950–2009

Figure 3a presents reconstructed spatial trend patterns over 1950–2009 for three cases: (1) EOFs from DRAKKAR/NEMO over 1958–2007—case 1, (2) EOFs from SODA over 1958–2007—case 2 and (3) EOFs from altimetry over 1993–2009—case 3 (here 15 modes are used for the reconstructions; this number of modes optimizes the results as discussed in Sect. 4.2).

Some features common to the two model-based reconstructions (cases 1 and 2) are seen in Fig. 3a; for example, the patterns in the Pacific, Indian, Austral and south Atlantic oceans. However, differences are noticed in the tropical Atlantic and North Atlantic south of Greenland. The altimetry-based reconstructed trends agree better with SODA (case 2)

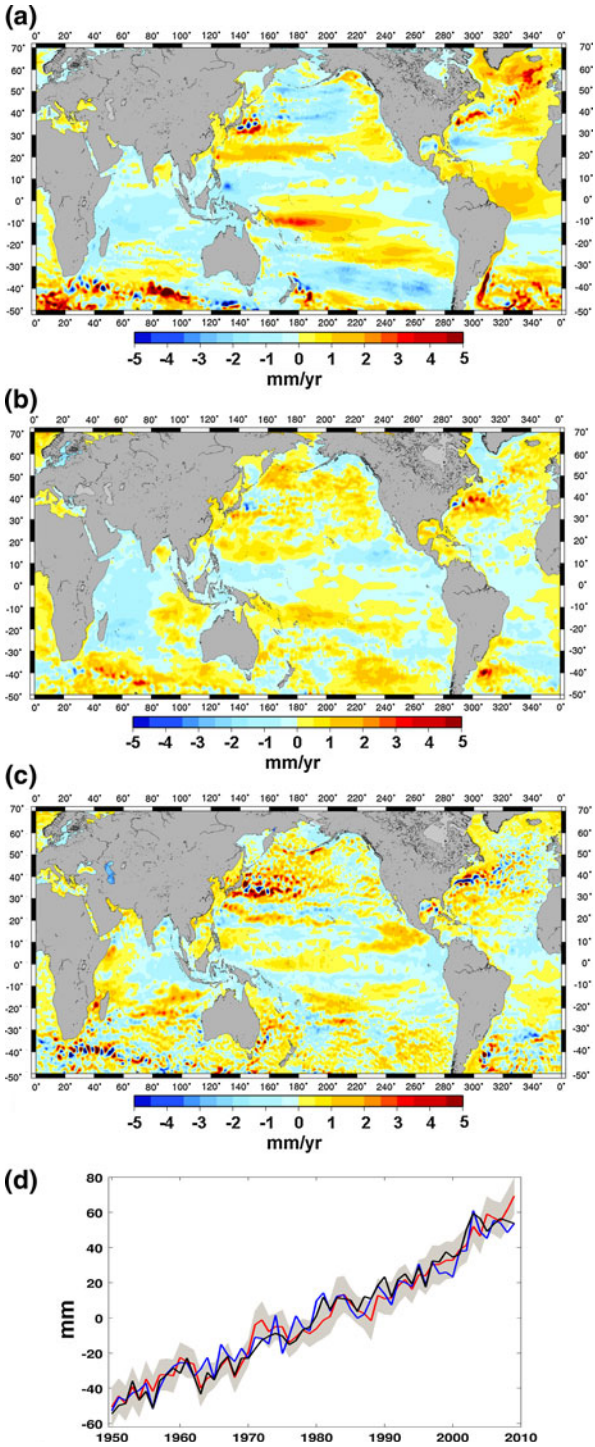

Fig. 3 Reconstructed spatial trends in sea level over 1950–2009 (15 first modes) based on: **a** EOFs of DRAKKAR/NEMO over 1958–2007, **b** EOFs of SODA over 1958–2007, **c** EOFs of satellite altimetry over 1993–2009. **d** The reconstructed global mean sea level since 1950 for the 3 reconstructions (*black curve* DRAKKAR/NEMO; *red curve* SODA; *blue curve* altimetry). The *grey shaded zone* represents the uncertainty of the altimetry-based reconstructed global mean sea level

than DRAKKAR/NEMO (case 1). We note that the DRAKKAR/NEMO reconstruction has locally higher amplitudes than the other two reconstructions.

Unlike the spatial patterns, the global mean sea level curves over 1950–2009 from the 3 reconstructions agree rather well (see Fig. 3d). Curves for the two model-based reconstructions (cases 1 and 2) fall within the uncertainty of the altimetry-based reconstructed sea level curve. This uncertainty was estimated from the quadratic sum of formal errors derived from the inversion process and tide-gauge data errors. The latter were estimated from a bootstrap method (Efron and Tibshirani 1993) for standard errors of yearly tide-gauge-based sea level values with a significance level—SL >95%. It dominates the total error.

The three global mean sea level curves present very similar trends over 1950–2009, 1.8 mm/year for the DRAKKAR/NEMO and altimetry-based reconstructions and 1.7 mm/year for the SODA-based reconstruction. Global mean interranual to decadal variability also correlates fairly well. The detrended global mean sea level from the DRAKKAR/NEMO-based reconstruction shows a correlation of 0.66 with the SODA-based reconstruction and 0.62 with the altimetry-based reconstruction.

We performed an EOF decomposition of the reconstructed grids over 1950–2009 for the three cases (note that the EOF decomposition of reconstructed sea level is not expected to be similar to that of the spatial input grids because new temporal amplitudes have been estimated). The global mean sea level was removed before the EOF decomposition. The 3 leading modes (EOF1/2/3) of each case (i.e. DRAKKAR-/NEMO-, SODA- and altimetry-based reconstructions) are shown in Fig. 4. The EOF1 temporal curves of the DRAKKAR-/NEMO- and altimetry-based reconstructions display an upward trend. For the DRAKKAR/NEMO reconstruction, the interranual variability of this curve correlates significantly (0.52 SL >99%) with the PDO index (e.g., Zhang et al. 1997) after $\sim$1975, showing an influence of the Pacific ocean on the leading mode over the last decades. It is not the case for the altimetry reconstruction because no similar significant correlation could be found with its EOF1 temporal curve. Noting that the spatial patterns of both EOF1 s closely resemble the trend patterns shown in Fig. 3, we conclude that this mode reflects the sea level signature of a low frequency signal. (of pseudo periodicity longer than the 60-year-long time span considered in this study). The EOF1 of the SODA reconstruction displays different characteristics. First, its temporal curve increases only after 1980, and second, its spatial pattern does not resemble the trend patterns shown in Fig. 3. Rather, it seems closer to an ENSO-like pattern. The temporal curve correlates well (0.62 with SL >99%) with the Southern Oscillation index (SOI) (difference of atmospheric pressure between Darwin, Australia, and Tahiti, French Polynesia: a proxy of ENSO), revealing the influence of ENSO. Unlike EOF1 s, EOF2 spatial patterns of the 3 reconstructions compare fairly well. Their temporal curves show significant influence from the Pacific region: EOF2 of the DRAKKAR/NEMO reconstruction correlates well with the PDO index before 1975 (0.65 with SL >99%), EOF2 of the SODA reconstruction correlates well with the SOI over 1950–2009 (0.67 with SL >99%) and EOF2 of the altimetry reconstruction correlates well with the PDO index over 1950–2009 (0.64 with SL >99%). Finally, EOF3s of the three reconstructions agree reasonably well each other. They all show significant correlation with the El Nino Modoki Index (EMI), a proxy of a different type of ENSO events marked by a warming of the central Pacific instead of the East Pacific (Ashok and Yamagata 2009). However, the correlation is reasonable for the DRAKKAR/NEMO reconstruction (0.54 with SL >99%) and weak for the SODA (0.30 with SL = 0.99%) and altimetry-based (0.34 with SL = 99%) reconstructions.

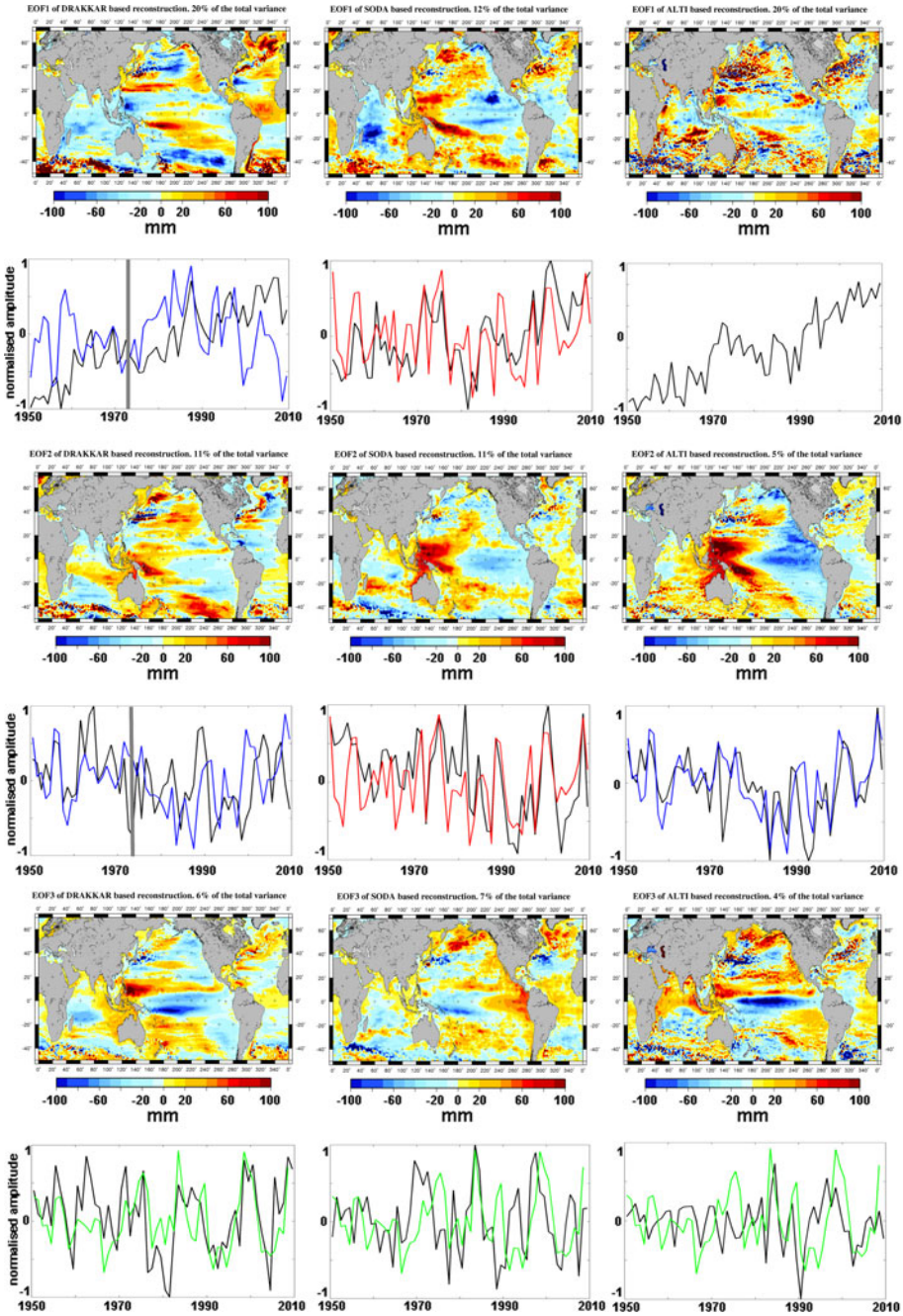

Fig. 4 EOFs modes 1 (*top panels*), 2 (*middle panels*) and 3 (*bottom panels*) of the reconstructed sea level heights based on EOFs of DRAKKAR/NEMO (1958–2007) (*left column*), SODA (1958–2007) (*middle column*) and altimetry (1993–2009) (*right column*). The global mean sea level was removed before the EOF decomposition. The reconstructions are based on 15 EOF modes. Superimposed to the temporal amplitudes (*black curves*) are plotted the PDO index (*blue*), the SOI index (*red*) and the EMI index (*green*)

Looking at Fig. 4, we note that DRAKKAR/NEMO- and altimetry-based reconstructions roughly capture similar signals, in particular a low-frequency signal. A similar low-frequency signal had been previously reported by Llovel et al (2009) in their sea level reconstruction over 1950–2003 using the OPA/NEMO ocean reanalysis (a version of the NEMO model with data assimilation; see Llovel et al. 2009 for details). The DRAKKAR/NEMO- and altimetry-based reconstructions also display in their EOF3 some imprint of the El Nino Modoki type event, in particular in recent years where the amplitude of the EOF3 gets higher. On the other hand, the SODA-based reconstruction seems to be dominated by the classical ENSO signal. It captures as well in its EOF3 some imprint of the El Nino Modoki type events, in particular in the recent years.

These three reconstructions use the same set of tide gauges but different input spatial grids. Thus, the differences noticed both in reconstructed spatial trend patterns and EOF decompositions likely reflect the dominant influence of these input spatial functions. Several factors may play a role, among them the quality of the sea level grids (e.g., the respective performance of the DRAKKAR/NEMO and SODA ocean models) and the period covered by the EOFs were used to do the reconstruction (50 years for DRAKKAR/NEMO and SODA, and 17 years for altimetry). We examine below the influence of the latter factor (in addition to that of the number of EOF modes used for the reconstruction).

4.2 Optimization of the Number of EOF Modes Used for the Reconstruction and Length of Input Sea Level Grids

In this section, we examine the effect of the number of EOF modes used for the reconstruction and the length of the input sea level grids. To find the optimal case, we perform two kind of comparisons: (1) we compare locally reconstructed and observed sea level time series over the time span of data availability at tide gauges not used in the reconstruction (91 reconstructions are completed, omitting one gauge at a time; we then compare at each corresponding site the reconstructed and observed sea level time series) and (2) we compare global reconstructed trends with (observed) altimetric trends over 1993–2009. For that purpose, we only consider the DRAKKAR/NEMO reconstruction. For the reconstruction, two parameters were varied: the number of modes (10, 15, 20, 25 and 30 modes were considered) and the length of the input grids to compute the EOFs (50 years, 40 years, 30 years and 20 years; the final year is always 2007, meaning that the time span of the input grids starts in 1958, 1968, 1978 and 1988, respectively).

Figure 5 shows the reconstructed trend maps over 1950–2009 with 50-year, 40-, 30- and 20-year long DRAKKAR/NEMO EOFs (with 15 and 20 modes). At global scale, these different reconstructions are consistent with each other except in the southern oceans south of 45°S. This region is actually not constrained by any tide gauge since the lowest latitude tide gauge we use is located at 44°S. For that reason, the reconstructed fields in the high latitude southern oceans are not very reliable. At regional scale, some discrepancies are noticed. The two reconstructions using 30- and 20-year long EOFs show a larger positive pattern in the southern tropical Pacific with lower amplitude than in the other reconstructions. It should be noticed as well that the 15-mode reconstructions based on 40- and 30-year long EOFs show a negative pattern south of Greenland that is not seen in the other reconstructions. To decide which case provides the best results, we present below different validations.

4.2.1 Validation with Independent Tide Gauges and Optimization of the Mode Number and EOF Length

Because in the reconstruction, we used all long, high-quality tide-gauge records available in the PSMSL data base, none were left for validation of the reconstruction. Thus, as in Llovel et al. (2009), we removed one by one each tide-gauge record, and then performed 91 new reconstructions with only 90 tide-gauge time series and compared at the left tide-gauge site reconstructed and observed sea level. Figure 6a shows the mean correlation between reconstructed time series and tide-gauge records over their overlapping time span as a function of input grid length and number of modes while Fig. 6b shows the standard deviation (rms) of the differences between reconstructed trends and tide-gauge trends over their overlapping time span. Both figures clearly show that 25-, 30- and 35-mode reconstructions perform less well than 10-, 15- and 20-mode reconstructions. We also note that the smallest rms is obtained for the longest input grid lengths (>40 years). The differences between 10 and 15 modes is very small but the 15-mode reconstruction seems to perform better in terms of reconstructed interannual variability since it shows slightly higher mean correlation with tide-gauge records when using long EOFs (see Fig. 6a). In the following, we consider 15 modes as optimal. In addition, reconstructions based on longest EOFs time span seem to perform better.

4.2.2 Validation with Altimetry Data Over the Altimetry Time Span (1993–2009)

Another method to validate the reconstructions and determine the optimal number of modes and EOF temporal length is to compare the reconstructed fields with observed (from altimetry) sea level over the altimetry time span (1993–2009). Mean correlation between reconstructed time series and observed time series over 1993–2009 at each grid mesh over the whole oceanic domain are shown in Fig. 6c as a function of number of modes and EOF temporal length. Root mean squares of the differences between reconstructed and observed trends over 1993–2009 at each grid mesh are also shown in Fig. 6d. As for the validation with tide gauges, we find that the highest mean correlation and lowest rms are obtained for 10–15–20 modes. In terms of trend rms, the impact of the EOF period is barely visible. In terms of mean correlation, we find here that on these short time scales (1993–2009), reconstructions with short EOF periods (<20 years) perform better. This is unlike the result obtained by comparison with independent tide gauges over the long period 1950–2009 (see Fig. 6a). But this is not surprising because these reconstructions are based on 20-year-long EOFs over 1988–2007 for which the modelled sea level coincides very well with altimetry used here for verification. Note that for long EOF periods (>40 years), best results in terms of both mean correlation and trend differences are obtained for the 10–15 modes reconstructions.

To summarize, the above comparisons indicate that the $\sim$15 mode case (i.e. between 10 and 20 modes) optimizes the reconstruction when the whole time span 1950–2009 is considered. This is due to the fact that higher modes contain more noise while small scale features can not be resolved during the inversion process because of the too sparse tide-gauge data. Hence, using too many modes makes the reconstructions noisy and increases artificially the amplitude of the regional variability. In addition, the 15-mode reconstructions are optimized when the input grids time is sufficiently long (roughly >30–40 years).

On the basis of the results shown on Fig. 6, the reconstruction that seems to give the best results is the 15-mode reconstruction based on 50-year long EOFs.

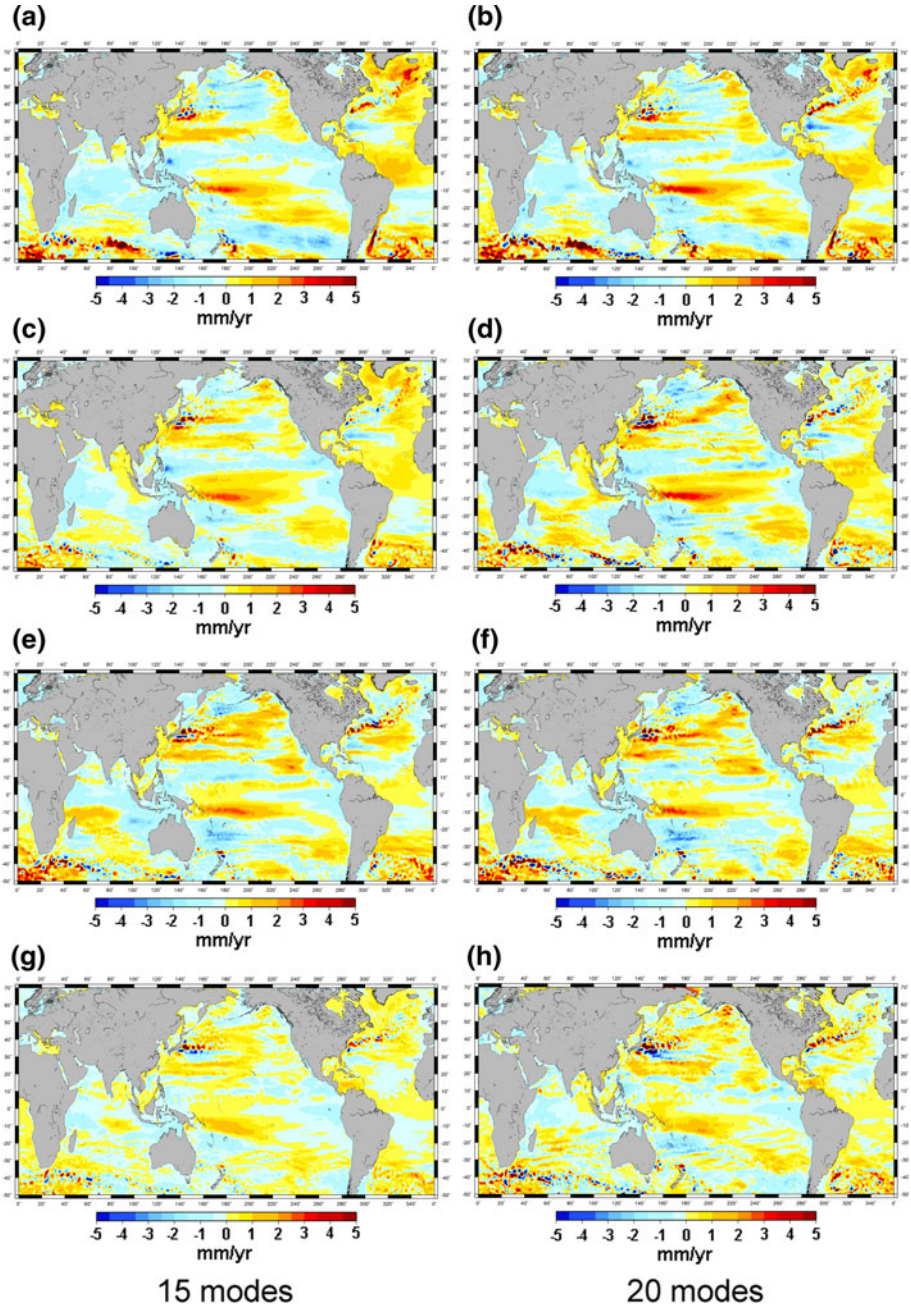

Fig. 5 Spatial trend patterns of the DRAKKAR/NEMO reconstruction (15 and 20 modes) for 50-year EOFS (**a** and **b**), 40-year EOFs (**c** and **d**), 30-year EOFs (**e** and **f**) and 20-year EOFs (**g** and **h**)

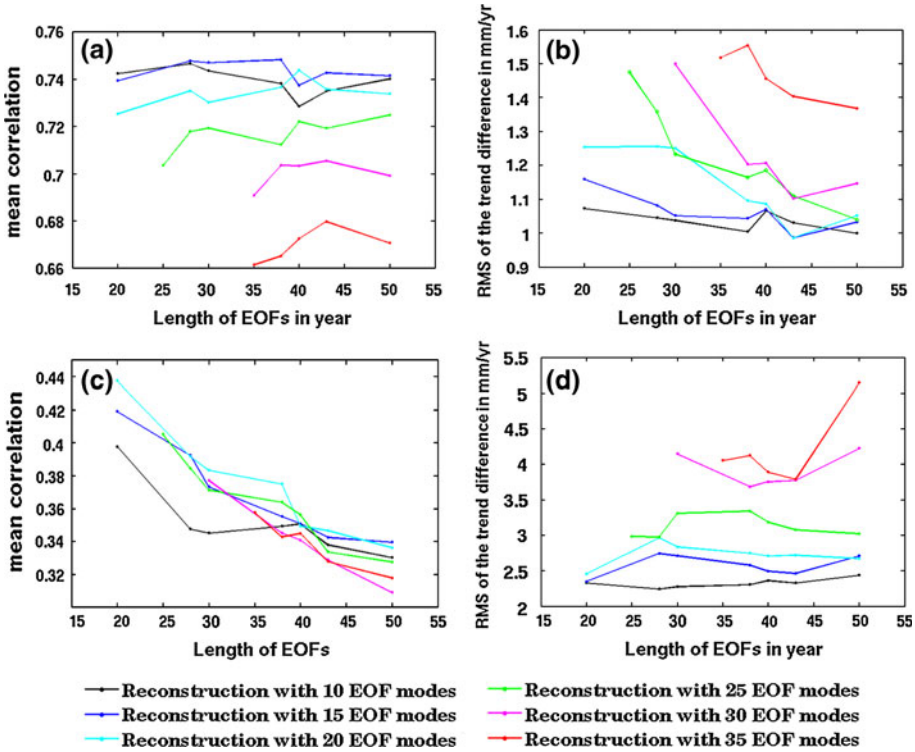

Fig. 6 *Top panels* correlation and rms trend differences between DRAKKAR/NEMO reconstructed sea level time series and each of the 91 tide gauges not used in the reconstruction (91 reconstructions are completed, omitting one gauge at a time; we then compare at each corresponding site the reconstructed and observed sea level time series), *bottom panels* correlation and trend differences between DRAKKAR/NEMO reconstructed sea level time series and altimetry. Results are presented for reconstructions using 10 modes (*black curves*), 15 modes (*blue curves*), 20 modes (*cyan curves*), 25 modes (*green curves*), 30 modes (*magenta curves*) and 35 modes (*red curves*). **a** Mean of the 91 correlations between tide gauges and DRAKKAR/NEMO reconstructed sea level time series over 1950–2009 at the tide-gauge location as a function of mode number and EOF length. **b** rms of the 91 differences between tide-gauge records not used in the reconstruction and DRAKKAR/NEMO reconstructed sea level trends over 1950–2009 at the tide-gauge location as a function of mode number and EOF length. **c** Mean of the correlations between satellite altimetry and DRAKKAR/NEMO reconstructed sea level time series over 1993–2009 as a function of mode number and EOF length (the correlations are computed over the 70°N–50°S oceanic domain on 1° × 1° grid meshes). **d** rms of the differences between satellite altimetry and DRAKKAR/NEMO reconstructed sea level trends over 1993–2009 as a function of mode number and EOF length (the differences are computed over the 70°N–50°S oceanic domain on 1° × 1° grid meshes)

4.3 Comparisons Between the Three Reconstructions (DRAKKAR/NEMO, SODA and Altimetry) Over 1950–2009

The results presented in Sect. 4.2 with the DRAKKAR/NEMO EOFs lead us to prefer the 15-mode and 50-year long input grids. A similar option is considered for the SODA input grids. For altimetry, we can only use 17-year long input grids (with 15 modes for the reconstruction). We can now compare the respective performances of these three cases. As for case 1 (DRAKKAR/NEMO EOFs), we compare the performances of the SODA and altimetry reconstructions at each of the 91 tide gauges not used in their respective reconstructions. Figure 7 left panels show histograms of the 91 correlations between

reconstructed and observed time series at tide gauges not used in the reconstruction. The high number of correlations higher than 0.7 (68) and of standard deviations lower than 30 mm (57) gives confidence in the reconstructed fields. The right panels show histograms of the rms differences between these time series. The top panel shows the DRAKKAR/NEMO reconstruction results, the middle one the SODA reconstruction results and the bottom panel the altimetry reconstruction results.

No clear conclusion can be drawn from Fig. 7, as no single case appears to perform better. We note that the SODA histograms spread more than DRAKKAR/NEMO and altimetry histograms but differences are not drastic. The DRAKKAR/NEMO and altimetry reconstructions give roughly similar performances. As noticed above for the EOF decomposition of the reconstructed sea level grids, the DRAKKAR/NEMO- and altimetry-based reconstructions compare better with each other than with the SODA-based reconstruction. The reason for this is unclear. Possibly, each case at its advantages and drawbacks. For example, the models provide longer input sea level grids (50 years compared with the 17-year long altimetry record), allowing better capture of the low-frequency variability. But the dominant modes of sea level variability remain imperfectly simulated by the models, whereas they are likely better reproduced by the altimetry data. In fact, these factors act in producing more or less similar reconstructions.

In Fig. 8 is shown the map of the absolute value of the differences between reconstructed spatial trend patterns over 1950–2009 with DRAKKAR/NEMO (EOFs over 1958–2007, 15 modes) and SODA (EOFs over 1958–2007, 15 modes). The difference signal is low in tropical regions (on the order of 1–2 mm/year) but much higher in the mid and high latitudes, as well as in areas of western boundary currents, likely a result of the poor performance of models in these regions. This is an illustration of less robust reconstructed results in these particular regions whatever the choice of the input model.

5 Mean Reconstruction Based on Averaging of the DRAKKAR/NEMO-, SODA- and Altimetry-Based Reconstructions; Comparison with Published Reconstructions

As classically done in climate modelling, we averaged the three reconstructions discussed above to provide a 'mean' reconstruction. This was done by averaging at each yearly time step the three reconstructed grids. Figure 9a shows spatial trend patterns over 1950–2009 of this 'mean' reconstruction, with the global mean trend (of 1.8 mm/year) included. Figure 9b shows the same map in which the global mean trend has been removed. Figure 9c shows the standard deviation (rms) of the spatial trend patterns of the 'mean' reconstruction. Low rms are observed almost everywhere, except in western boundary current regions, south of Iceland and south-east of Papua New-Guinea . In these areas, the reconstructed signal should be taken with caution, as indicated above.

We compared the spatial trend patterns of our 'mean' reconstruction with those from Hamlington et al. (2011) based on cyclostationary functions. Over the altimetry period, the reconstructed patterns are very similar (and in good agreement with altimetry observations). However, over longer time spans (1950–2001), the patterns look quite different (see Fig. 6 of Hamlington et al. 2011). The exact cause of such a discrepancy, possibly due to the choice of the basis functions, remains to be investigated.

Figure 10 shows the global mean sea level over 1950–2009 based on the 'mean' reconstruction. Its trend amounts to 1.8 ± 0.1 mm/year. The 0.1 mm/year uncertainty is the formal error. A more realistic error is likely closer to 0.3–0.4 mm/year (e.g., Ray and Douglas 2011 and Church and White 2011 propose a mean trend error of 0.26 and 0.4 mm/

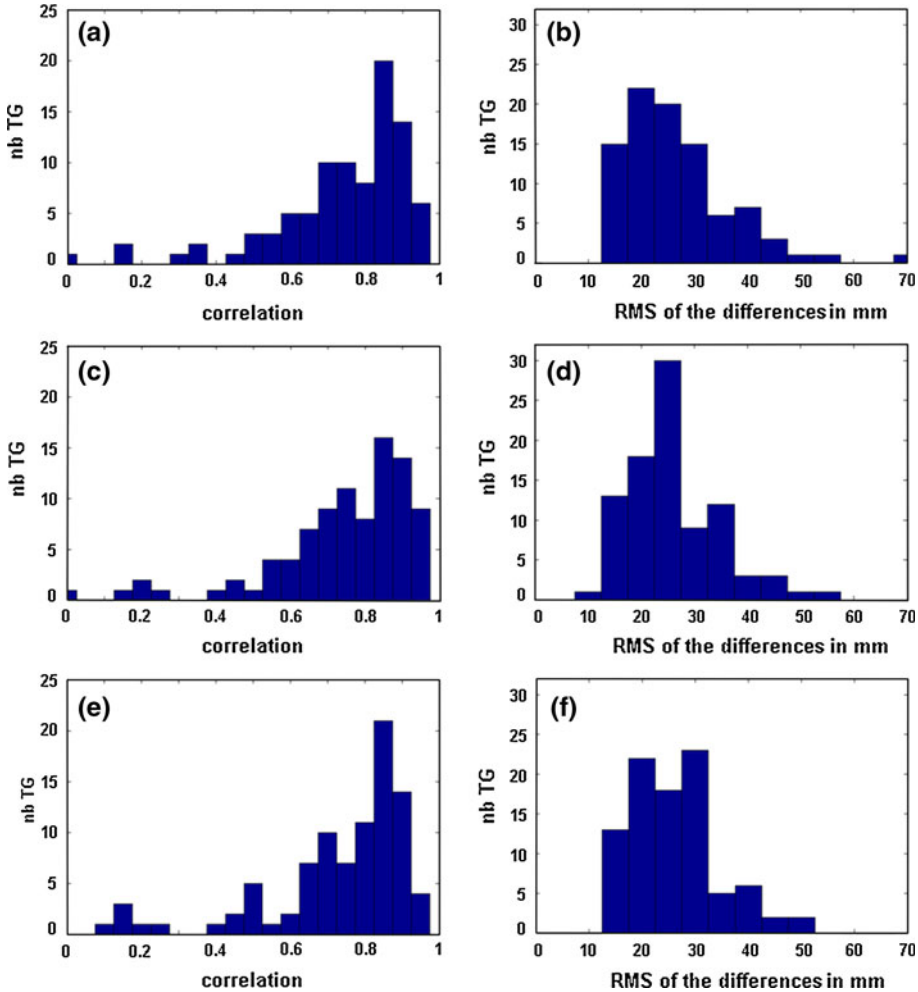

Fig. 7 Performance of the 15-mode reconstructions: (*left*) histogram of the correlations between observed and reconstructed sea level time series at tide-gauge sites not used in the reconstruction (91 sites considered); (*right*) histogram of rms difference (observed minus reconstructed) time series at the tide-gauge locations. **a** and **b** are for the DRAKKAR/NEMO reconstruction (EOFs over 1958–2007, 15 modes) while **c** and **d** are for the SODA reconstruction (EOFs over 1958–2007, 15 modes). **e** and **f** are for the altimetry-based reconstruction (EOFs over 1993–2009, 15 modes)

year, respectively, after accounting for various sources of errors, including GIA uncertainty).

Other published estimates of global mean sea level curves—either based on the reconstruction approach as described here or on other methods—are available in the literature (e.g., Chambers et al. 2002a, b; Church et al. 2004; Holgate 2007; Jevrejeva et al. 2006, 2008; Wenzel and Schroeter 2010; Church and White 2011; Ray and Douglas 2011; Hamlington et al. 2011). In Fig. 10, we have superimposed the global mean sea level curves based on the Church and White (2011) and Hamlington et al. (2011) reconstructions. The global mean sea level from our 'mean' reconstruction agrees very well with that from Church and White (2011) (within the uncertainty computed here as for Fig. 3d), both

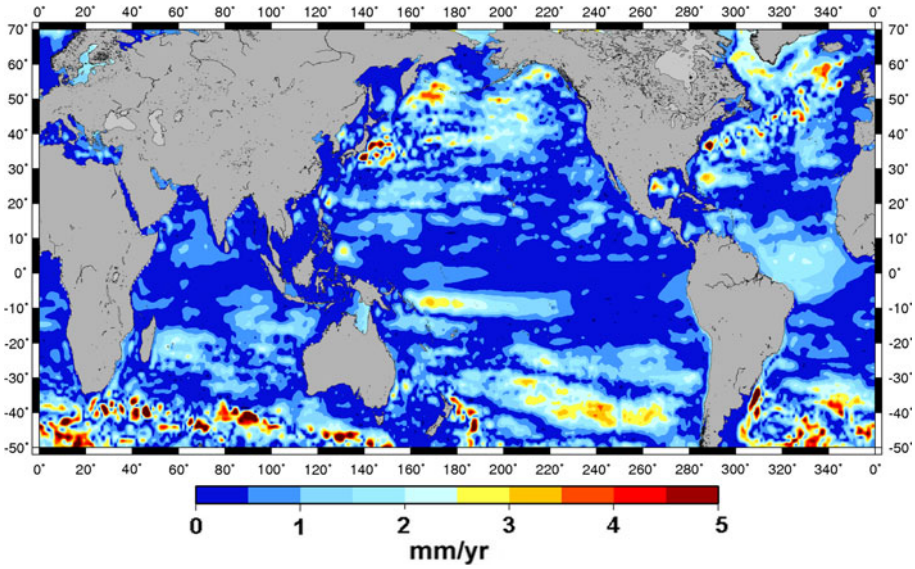

Fig. 8 Map of the absolute value of the differences between reconstructed spatial trend patterns over 1950–2009 with DRAKKAR/NEMO (EOFs over 1958–2007, 15 modes) and SODA (EOFs over 1958–2007, 15 modes)

in terms of interannual variability and trends (a trend of 1.8 mm/year is found with the Church and White data over 1950–2009). The agreement with the Hamlington et al. (2011) curve is not as good. The latter shows a larger trend of 1.95 ± 0.4 mm/year and slightly less interannual variability. Again, the difference may result from the choice of the basis functions.

Overall, the global mean sea level trend of our 'mean' reconstruction is very comparable to most previously published estimates for the second-half twentieth century. For the whole twentieth century, Ray and Douglas (2011)'s reconstruction proposes a value of 1.7 ± 0.26 mm/year quite similar to Church and White (2011) (equal to 1.7 ± 0.2 mm/year for 1900–2009). From a neuronal network technique, Wenzel and Schroeter (2010) found a trend of 1.6 ± 0.25 mm/year between 1900 and 2006.

6 Discussion

In this study, we developed and compared different 2-D sea level reconstructions based on the EOF approach, using different spatial grids as input. An EOF analysis of the reconstructed sea level fields shows a dominant low-frequency signal related to the PDO. Other leading modes are also related to other natural ocean modes, in particular ENSO.

Validation tests dedicated to estimate the influence of the number of EOF modes used for the reconstruction and the period of the input grids show that between 10 and 20 modes and input grids longer than 30–40 years optimize the results. The latter result is not really surprising as it is expected that the longer the input gridded data, the more complete the set of ocean modes of variability be accounted for in the reconstructed signal. The use of 50-year long OGCM grids to compute the input EOFs allows capturing low-frequency

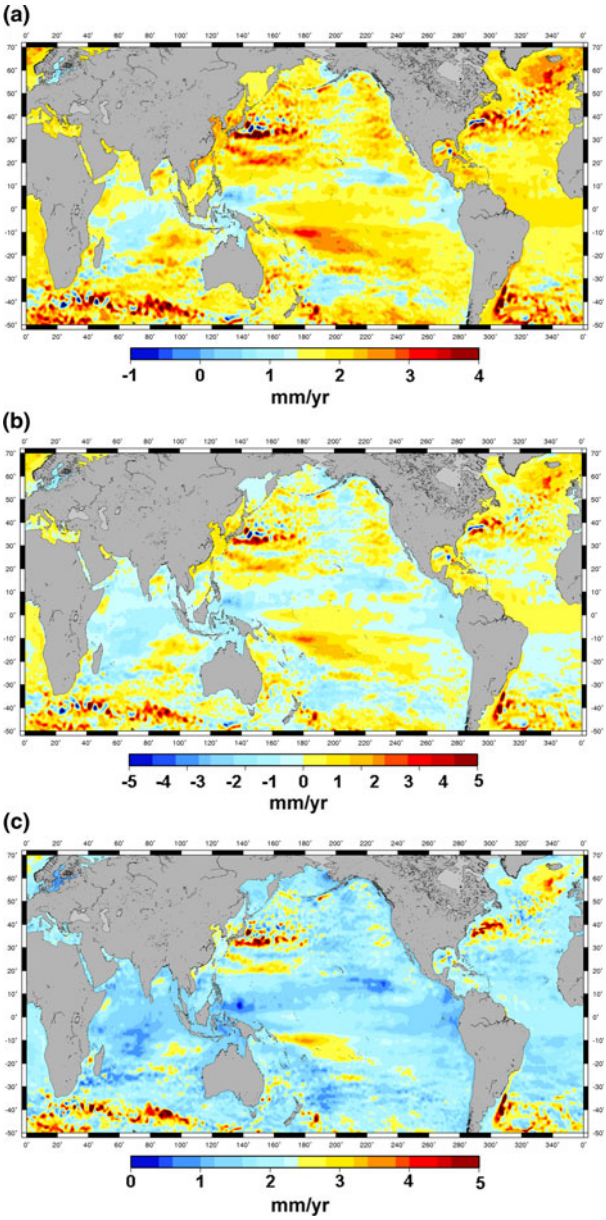

Fig. 9 Mean of the three reconstructions based on DRAKKAR (15 modes, EOF over 1958–2007), SODA (15 modes, EOF over 1958–2007) and altimetry. **a** Trends of the 'mean' reconstruction over 1950–2009. **b** Trends of the 'mean' reconstruction over 1950–2009. The global trend of 1.8 mm/year has been removed. **c** Standard deviation of the trends of the three reconstructions

modes of variability, in particular those related to the PDO. A similar conclusion was drawn by Llovel et al. (2009). However, the results presented above show that the spatial patterns of the reconstructed sea level are influenced by the input spatial grids (see Fig. 8).

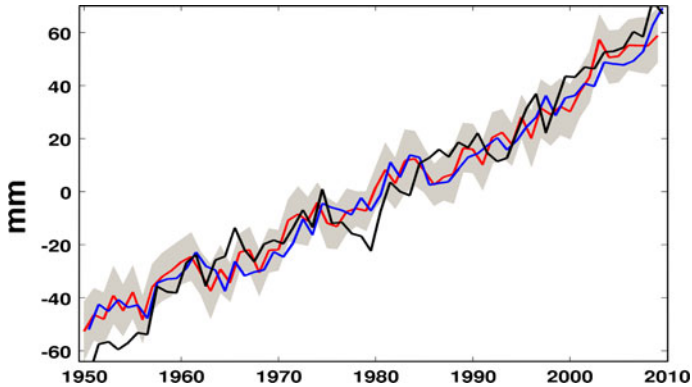

Fig. 10 Global mean sea level from the 'mean' reconstruction over 1950–2009 (*red curve*). We have added the reconstructed global mean sea level over 1950–2009 from Church et al. (2011) (*blue curve*) and Hamlington et al. (2011) (*black curve*). The grey shaded zone represents the uncertainty of the 'mean' reconstructed global mean sea level

The assessment performed in this study also showed that the DRAKKER/NEMO model-based and altimetry-based reconstructions compare rather well with each other (see Fig. 4). This is somewhat unexpected because the altimetry-based reconstruction uses only 17-years of input sea level grids. We interpret this as the result of some kind of compensation between longer input grids (from the model) and a better representation of the sea level variability (from the altimetry data). As a result, more or less similar reconstructions are obtained. Evidently, the best results are to be expected when 50 years of satellite altimetry will be available!

An interesting point is that the reconstructed global mean sea level is fairly independent of the input grids (see Fig. 3d). It appears also relatively independent of the tide-gauge selection. Indeed, we find a reconstructed global mean sea level very close to the Church and White (2011) one based on a different tide-gauge records selection.

Finally, one may wonder whether reconstructing past sea level has any interest provided that several OGCM outputs and ocean reanalyses now available are regularly improving and provide gridded sea level time series since the late 1950 s. While there is no doubt that ocean models improved much in the recent years, some differences are still observed between the models. This is illustrated in Fig. 11 showing the spatial trend difference map over 1958–2007 between DRAKKAR/NEMO and SODA. As for Fig. 8, we note that the difference signal is low in the tropics (on the order of only 1–2 mm/year) but higher in middle and high latitudes, probably reflecting that OGCMs and ocean reanalyses are still imperfect in these regions. Another argument to perform past 2-D sea level reconstructions is the fact that regional variability due to non-steric factors affects sea level. OGCMs and ocean reanalyses simulate steric variability only but not circulation changes due to land water mass addition or GIA or other mass redistribution effects causing solid Earth deformation and gravitational effects. To illustrate this, Fig. 12 shows the spatial trend difference map between the DRAKKAR model outputs over 1993–2007 and observed (altimetry-based) sea level over the same time span. Of course, the residual map seen in Fig. 12 may reflect model uncertainty, but we cannot exclude it also may well contain physical signal of non-steric origin present in the altimetry data but not in the model.

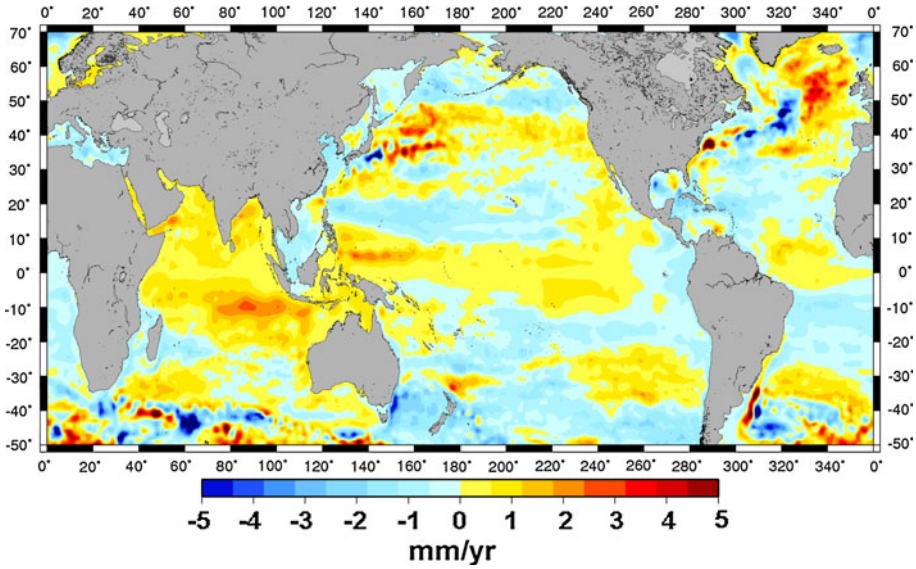

Fig. 11 Spatial trend pattern differences over 1958–2007 between DRAKKAR/NEMO model and SODA reanalysis

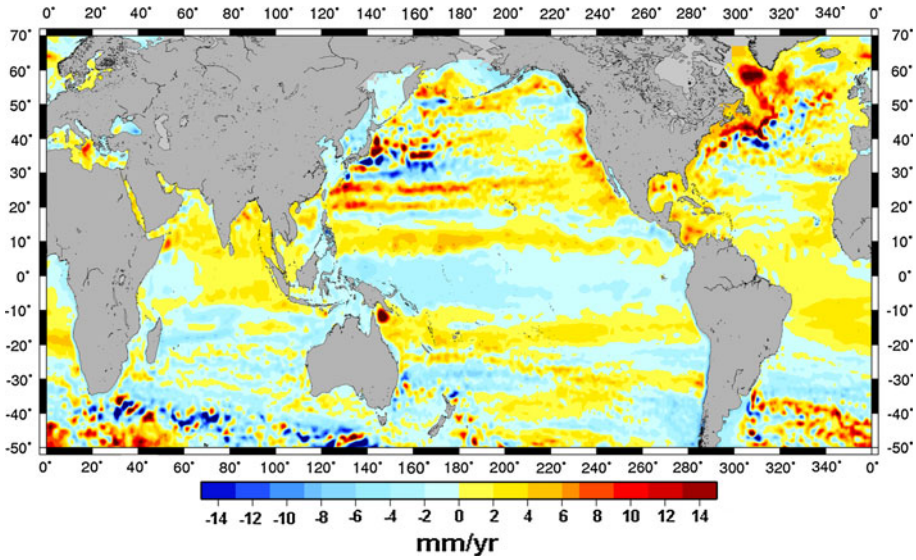

Fig. 12 Spatial trend pattern differences over 1993–2007 between DRAKKAR/NEMO model and altimetry-based sea level

Efforts to develop 2-D past sea level reconstructions are certainly worthwhile pursuing. However, as we have seen in this study, the reconstructed spatial trend patterns are somewhat dependent on the input spatial grids and basis functions. Using a larger number of tide-gauge data with improved spatial coverage may partly solve this problem. But the

tide-gauge coverage will never be good enough to capture all the sea level regional variability.

A potential solution of improvement is to perform 2-D reconstructions with an ensemble of input spatial grids (from different OGCMs and reanalyses) and then deduce a 'mean' reconstruction by averaging the different reconstructions, as done with coupled climate model projections of future regional sea level variability. In this study, we make a first attempt in this direction and produce a 'mean' reconstruction based on averaging reconstructed annual sea level grids from three independent reconstructions. This is a promising solution that should provide more and more realistic past sea level data when a larger set of reconstructions will be available.

Acknowledgments We thank two anonymous reviewers for their useful comments. M. Becker is supported by an ANR CNRS grant number ANR-09-CEP-001-01 (CECILE project). W. Llovel is supported by a NASA Postdoctorate fellowship. The 'mean' reconstructed sea level grids from the present study are available on request.

References

Ablain M, Cazenave A, Valladeau G, Guinehut S (2009) A new assessment of the error budget of global mean sea level rate estimated by satellite altimetry over 1993–2008. Ocean Sci 5:193–201

Altamimi Z, Collilieux X, Legrand J, Garayt B, Boucher C (2007) ITRF2005: a new release of the international terrestrial reference frame based on time series of station positions and earth orientation parameters. J Geophys Res 112:B09401. doi:10.1029/2007JB004949

Ashok K, Yamagata T (2009) Climate change: the El Niño with a difference. Nature 461:481–484. doi:10.1038/461481a

Barnier B, Madec G, Penduff T, Molines JM, Treguier AM, Le Sommer J, Beckmann A, Biastoch A, Böning C, Dengg J et al (2006) Impact of partial steps and momentum advection schemes in a global ocean circulation model at eddy-permitting resolution. Ocean Dyn 56:543–567

Berge-Nguyen M, Cazenave A, Lombard A, Llovel W, Viarre J, Cretaux JF (2008) Reconstruction of past decades sea level using thermosteric sea level, tide gauge, satellite altimetry and ocean reanalysis data. Glob Planet Change 62:1–13

Bonett DG, Wright TA (2000) Sample size requirements for estimating pearson, kendall, and spearman correlations. Psychometrica 65(1):23–28

Brodeau L, Barnier B, Treguier AM, Penduff T, Gulev S (2010) An ERA40-based atmospheric forcing for global ocean circulation models. Ocean Model 31:88–104

Calafat FM, Gomis D (2009) Reconstruction of Mediterranean sea level fields for the period 1945–2000. Glob Planet Change 66:225–234

Carrere L, Lyard F (2003) Modeling the barotropic response of the global ocean to atmospheric wind and pressure forcing—comparisons with observations. Geophys Res Lett 6:1275. doi:10.1029/2002GL016473

Carton JA, Giese BS (2008) A reanalysis of ocean climate using simple ocean data assimilation (SODA). Mon Weather Rev 136:2999–3017

Cazenave A, Llovel W (2010) Contemporary sea level rise. Annu Rev Mar Sci 2:145–173

Chambers DP, Mehlhaff CA, Urban TJ, Nerem RS (2002a) Analysis of interannual and low-frequency variability in global mean sea level from altimetry and tide gauges. Phys Chem Earth 27:1407–1411

Chambers DP, Mehlhaff CA, Urban TJ, Fuji D, Nerem RS (2002b) Low-frequency variations in global mean sea level: 1950–2000. J Geophys Res 107(C4):3026. doi:10.1029/2001JC001089

Christiansen B, Schmith T, Thejll P (2010) A surrogate ensemble study of sea level reconstructions. J Clim 23:4306–4326

Church JA, White NJ (2006) A 20th century acceleration in global sea-level rise. Geophys Res Lett 33:L01602. doi:10.1029/2005GL024826

Church JA, White NJ (2011) Changes in the rate of sea-level rise from the late 19th to the early 21st century. Surv Geophys 1–18. doi:10.1007/s10712-011-9119-1

Church JA, White NJ, Coleman R, Lambeck K, Mitrovica JX (2004) Estimates of the regional distribution of sea-level rise over the 1950 to 2000 period. J Clim 17(13):2609–2625

Church JA, White NJ, Konikow LF, Domingues CM, Cogley JG, Rignot E, Gregory JM, van den Broeke MR, Monaghan AJ, Velicogna I (2011) Revisiting the earth's sea level and energy budgets from 1961 to 2008. Geophys Res Lett. doi:10.1029/2011GL048794

DRAKKAR Group (2007) Eddy-permitting ocean circulation hindcasts of past decades. Clivar Exch 12(3):8–10

Dussin R, Treguier AM, Molines JM, Barnier B, Penduff T, Brodeau L, Madec G (2009) Definition of the interannual experiment ORCA025-B83, 1958–2007. LPO Report 902

Efron B, Tibshirani RJ (1993) An Introduction to the bootstrap. Chapman & Hall, New York

Greatbatch RJ (1994) A note on the representation of steric sea-level in models that conserve volume rather than mass. J Geophys Res 99:12767–12771

Hamlington BD, Leben R, Nerem S, Han W, Kim KY (2011) Reconstructing sea level using cyclostationary empirical orthogonal functions. J Geophys Res. doi:10.1029/2011JC007529

Holgate S (2007) On the decadal rates of sea level change during the twentieth century. Geophys Res Lett 34:L01602. doi:10.1029/2006GL028492

Jevrejeva S, Grinsted A, Moore JC, Holgate S (2006) Nonlinear trends and multiyear cycles in sea level records. J Geophys Res 111:C09012. doi:10.1029/2005JC003229

Jevrejeva S, Moore JC, Grinsted A, Woodworth PL (2008) Recent global sea level acceleration started over 200 years ago? Geophys Res Lett 35:L08715. doi:10.1029/2008GL033611

Jourdan D, Balopoulos E, Garcia-Fernandez MJ, Maillard C (1998) Objective analysis of temperature and salinity historical data set over the Mediterranean Basin, IEEE

Kalnay EC, Kanamitsu M, Kistler R, Collins W, Deaven D, Gandin L, Iredell M, Saha S, White G, Woollen J et al (1996) The NCEP/NCAR 40-year reanalysis project. Bull Am Meteorol Soc 77:437–472

Kaplan A, Cane MA, Kushnir Y, Clement AC, Blumenthal MB, Rajagopalan B (1998) Analyses of global sea surface temperature 1856–1991. J Geophys Res 103:18567–18589

Kaplan A, Kushnir Y, Cane MA (2000) Reduced space optimal interpolation of historical marine sea level pressure: 1854–1992. J Clim 13:2987–3002

Kohl A, Stammer D (2008) Decadal sea level changes in the 50-year GECCO ocean synthesis. J Clim 21:1876–1890

Large W, Yeager S (2004) Diurnal to decadal global forcing for ocean and sea ice models: the datasets and flux climatologies, NCAR Tech. Note NCAR/TN460 + STR, Natl Cent for Atmos Res, Boulder, Colorado

Levitus S, Antonov J, Boyer T (2005) Warming of the world ocean, 1955–2003. Geophys Res Lett 32:L02604. doi:10.1029/2004GL021592

Llovel W, Cazenave A, Rogel P, Lombard A, Bergé-Nguyen M (2009) Two-dimensional reconstruction of past sea level (1950–2003) from tide gauge data and an Ocean General Circulation Model. Clim Past 5:217–227

Lombard A, Cazenave A, Le Traon PY, Ishii M (2005) Contribution of thermal expansion to present-day sea level rise revisited. Glob Planet Change 47:1–16

Lombard A, Garric G, Penduff T (2009) Regional patterns of observed sea level change: insights from a 1/4A degrees global ocean/sea-ice hindcast. Ocean Dyn 59(3):433–449

Madec G (2008) NEMO reference manual, ocean dynamics component: NEMO-OPA. Preliminary version. Note du Pole de modélisation, Institut Pierre-Simon Laplace (IPSL), France, pp 1288–1619

Meyssignac B, Salas y Melia D, Becker M, Llovel W, Cazenave A (2011a) Tropical Pacific spatial trend patterns in observed sea level: internal variability and/or anthropogenic signature? Clim Past (in review)

Meyssignac B, Calafat SM, Somot S, Rupolo V, Stocchi P, Llovel W, Cazenave A (2011b) Two-dimensional reconstruction of the Mediterranean sea level over 1970–2006 from tide gauge data and regional ocean circulation model outputs. Glob Planet Change 77:49–61

Milne G, Gehrels WR, Hughes C, Tamisiea M (2009) Identifying the causes of sea level changes. Nat Geosci 2:471–478

Mitrovica JX, Gomez N, Clark PU (2009) The sea-level fingerprint of West Antarctic collapse. Science 323:753

Moore JC, Jevrejeva S, Grinsted A (2011) The historical sea level budget. Ann Glaciol 52959

Nerem RS, Chambers DP, Choe C, Mitchum GT (2010) Estimating mean sea level change from the TOPEX and Jason altimetermissions. Mar Geodesy 33(1):435–446

Nicholls RJ (2010) Impacts of and responses to sea level rise. In: Church J, Woodworth P, Aarup T, Wilson WS (eds) Understanding sea level rise and variability. Wiley-Blackwell, New York

Peltier WR (2004) Global glacial isostasy and the surface of the ice-age earth: the ICE-5G (VM2) model and GRACE. Annu Rev Earth Planet Sci 32:111–149

Penduff T, Juza M, Brodeau L, Smith G, Barnier B, Molines J, Treguier A, Madec G (2010) Impact of global ocean model resolution on sea-level variability with emphasis on interannual time scales. Ocean Sci 6:269–284

Preisendorfer RW (1988) Principal component analysis in meteorology and oceanography. Developments in atmospheric science, vol 17. Elsevier, Amsterdam

Ray R, Douglas B (2011) Experiments in reconstructing twentieth-century sea levels. Prog Oceanogr 91: 496–515

Rosner B (1975) On the detection of many outliers. Technometrics 17:221–227

Stammer D (2008) Response of the global ocean to Greenland and Antarctica melting. J Geophys Res 113:C06022. doi:10.1029/2006JC001079

Stammer D, Agarwal N, Herrmann P, Kohl A, Mechoso CR (2011) Response of a coupled ocean-atmosphere model to Greenland melting. Surv Geophys 32:621–642. doi:10.1007/s10712-011-9142-2

Steele M, Morley R, Ermold W (2001) PHC: a global ocean hydrography with a high quality Arctic Ocean. J Clim 14:2079–2087

Toumazou V, Cretaux JF (2001) Using a Lanczos eigensolver in the computation of empirical orthogonal functions. Mon Weather Rev 129:1243–1250

Uppala SM, da CostaBechtold V, Fiorino M, Gibson JK, Haseler J, Hernandez A, Kelly GA, Li X, Onogi K, Saarinen S, Sokka N, Allan RP, Andersson E, Arpe K, Balmaseda MA, Beljaars ACM, van de Berg L, Bidlot J, Bormann N, Caires S, Chevallier F, Dethof A, Dragosavac M, Fisher L, Fuentes M, Hagemann S, Hólm E, Hoskins BJ, Isaksen L, Janssen PAEM, Jenne R, McNally AP, Mahfouf J-F, Morcrette JJ, Rayner NA, Saunders RW, Simon P, Sterl A, Trenberth KE, Untch A, Vasiljevic D, Viterbo P, Woollen J (2005) The ERA-40 re-analysis. Q J Roy Meteorol Soc 131:2961–30128

Wenzel M, Schroeter J (2010) Reconstruction of regional mean sea level anomalies from tide gauges using neural networks. J Geophys Res 115:C08013. doi:10.1029/2009JC005630

Woodworth PL, Player R (2003) The permanent service for mean sea level: an update to the 21st century. J Coastal Res 19:287–295

Woppelmann G, Letetrel C, Santamaria A, Bouin MN, Collilieux X, Altamimi Z, Williams SDP, Martin Miguez B (2009) Rates of sea-level change over the past century in a geocentric reference frame. Geophys Res Lett 36:L12607. doi:10.1029/2009GL038720

Wunsch C, Ponte RM, Heimbach P (2007) Decadal trends in sea level patterns: 1993–2004. J Clim. doi: 10.1175/2007JCLI1840.1

Zhang Y, Wallace JM, Battisti DS (1997) ENSO-like interdecadal variability: 1900–93. J Clim 10: 1004–1020